High T_c superconductivity at the interface between an insulating Infinite Layers Cuprate and $SrTiO_3$

D. Di Castro[1,2,*], C. Cantoni[3], F. Ridolfi[1], C. Aruta[2], A. Tebano[1,2], N. Yang[2,4], G. Balestrino[1,2]

[1]*Dipartimento di Ingegneria Civile e Ingegneria Informatica, Università di Roma Tor Vergata, Via del Politecnico 1, I-00133 Roma, Italy*

[2]*CNR-SPIN, Università di Roma Tor Vergata, Roma I-00133, Italy*

[3]*Materials Science and Technology Division, Oak Ridge National Laboratory, Oak Ridge, TN 37831-6116, USA*

[4]*Facoltà di Ingegneria, Università degli studi Niccolò Cusano, Rome I-00166, Italy*

At interfaces between complex oxides it is possible to generate electronic systems with unusal electronic properties, which are not present in the isolated oxides. One important example is the appearance superconductivity at the interface between insulating oxides, although, up to now, only with very low T_c. Here we report the occurrence of *high* T_c superconductivity in the bilayer $CaCuO_2/SrTiO_3$, where both the constituent oxides are insulating. The $CaCuO_2/SrTiO_3$ interface must be realized between the Ca plane of $CaCuO_2$ and the TiO_2 plane of $SrTiO_3$. Only in this case extra oxygen ions can be incorporated in the interface Ca plane, acting as apical oxygen for Cu and providing holes to the CuO_2 planes. A detailed hole doping spatial profile has been obtained by STEM/EELS O K-edge, clearly showing that the (super)conductivity is confined to about 1-2 $CaCuO_2$ unit cells close to the interface with $SrTiO_3$. The results obtained for the $CaCuO_2/SrTiO_3$ interface can be extended to multilayered high T_c cuprates, answering some open questions related to these systems.

The interface between complex transition metal oxides is recently emerging as one of the most interesting systems in condensed matter physics [1]. Indeed, a range of fascinating interface electronic phenomena, as a high mobility two-dimensional (2D) electron gas, quantum Hall effect, and superconductivity, have all been discovered in oxide hererostructures [2, 3, 4, 5, 6], but are absent in either of their constituents. In recent years, significant progress has been achieved in exploring the fundamental properties of such interfaces, and it has become clear that these electron systems offer the potential for possible future devices. One interesting example is the formation of conducting quasi–two-dimensional electron gas at the interface between the insulating perovskites $LaAlO_3$ and $SrTiO_3$ [1]. Strikingly, this interface is also superconducting at low temperature (about 10^{-1} K) [4,7].

On the other hand, the layered structure of cuprate high transition temperature superconductors (HTS) can be schematized as a sequence of natural interfaces between two blocks with different structure and functionality: an insulating block with infinite layer (IL) structure, containing the CuO_2 planes, and a charge reservoir (CR) block, that, opportunely doped by chemical substitution or excess oxygen ions, provides charge carriers to the IL block, giving rise to high transition temperature (T_c) superconductivity. The extraordinary electronic property shown by the interface between two insulating oxides, as in LAO/STO heterostructures, thus suggested the opportunity to exploit the conducting interface as a charge reservoir to dope a cuprate with IL structure, and thus to pump up the T_c from ~ 10^{-1} K to ~ 10^2 K. We have explored such a possibility by tailoring artificial superlattices $[(CaCuO_2)_n/(SrTiO_3)_m]_N$, made by N repetitions of the $(CaCuO_2)/(SrTiO_3)$ interface, where n and m are the number of unit cells of $CaCuO_2$ (CCO) and $SrTiO_3$ (STO), respectively [6, 8]. This system, is a high T_c superconductor (T_c = 50 K) where CCO, an insulating cuprate with the "infinite layer" structure, has been used instead of LAO to be coupled to STO. The overall experimental studies we have conducted on these superlattices have suggested that the superconductivity is mainly confined at the interface between CCO and STO [6, 8-10]. Here we present a detailed, atomic-scale study of the

CCO/STO interface, which is of paramount importance, since, differently from previous cuprate/cuprate heterostructures [5, 11, 12], now the spacer between the superconducting blocks is not a cuprate, but it is STO, and the CCO/STO interfaces are thus very similar to the IL/CR native interface of HTS. The results obtained from the investigation of the CCO/STO interface can be used to extract important information on the physical processes occurring in HTS.

A detailed study of the CCO/STO interface can be conducted on $(CCO)_n/(STO)_m$ bilayers, that is, a heterostructure made by a relatively thick layer of CCO ($n \approx 10 \div 60$ unit cells) and a relatively thick layer of STO ($m \approx 10 \div 60$ unit cells) stacked along the *c*-axis. In this work, we show that a single CCO/STO interface, present in the bilayers, still show high T_c superconductivity, with the highest T_c about 40 K, a value smaller, but still comparable with those found in the CCO/STO superlattices [6, 8]. By using state-of-the-art aberration-corrected scanning transmission electron microscopy (STEM) coupled to electron energy loss spectroscopy (EELS), we give a *direct* evidence that the "charge reservoir" consists of a *single* CaO_x atomic plane of CCO at the interface with the TiO_2 plane of STO, where O_x indicates the presence of extra oxygen ions. STEM/EELS O K-edge spectra show that the doping holes, coming from the oxygen doped plane at the interface, extend over nearly one-two CCO unit cells from the interface, giving rice to a pure interface superconductivity. Given the particular structure of the constituent oxides, the results obtained on CCO/STO heterostructure can be used to explain unsolved questions in standard HTS.

Results

We used the pulsed laser deposition technique to synthesize the CCO/STO bilayers. The films were deposited on NdO terminated 5x5 mm^2 $NdGaO_3$ (110) (NGO) oriented mono-crystalline substrates, which have been shown to be the most suitable substrate to grow the CCO [13] and CCO/STO superlattices [8]. A large number (hundreds) of CCO/STO heterostructures have been grown by

varying the growth oxidizing conditions, the thickness and the stacking order of the constituent blocks. All these parameters matter for the occurrence of the superconducting phase.

In Fig.1 the Co K_α x-ray diffraction spectrum of a typical CCO/STO bilayer on NGO substrate is shown. Both the (001) and (002) peaks of CCO are clearly visible, whereas only the (002) peak of the STO is present, since the (001) overlaps with the much more intense 001 peak of the pseudocubic crystallographic structure of the NGO substrate. The CCO and STO blocks of this sample are 60 and 50 unit cells thick, respectively, as evinced by the XRD finite size oscillations shown in the panel c) and d) of the same figure. The finite size oscillations have been measured in all the samples with CCO and STO blocks thicker than about 12 unit cells. The thickness of thinner CCO blocks has been deduced by using the deposition rate obtained for thicker blocks, and then confirmed by STEM images. The image reported in panel d) of Fig.1 shows a typical $(CaCuO_2)/(SrTiO_3)$ bilayer and confirms the good structural quality of both the CCO and STO blocks and the sharpness of the CCO/STO interface.

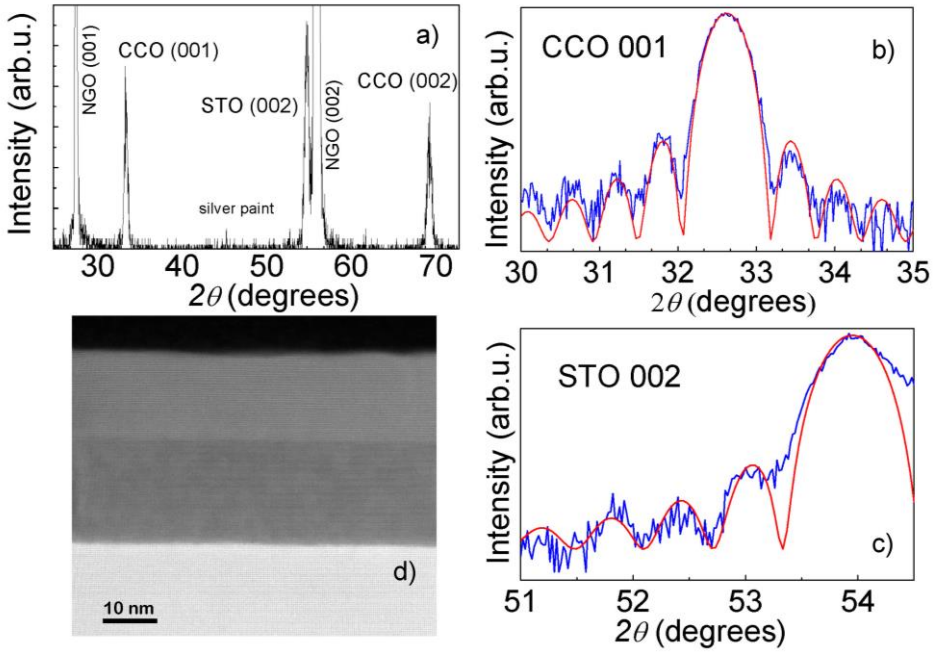

Figure 1: **Structural characterization of the bilayer CCO/STO**. a) XRD spectrum which shows the (00l) and (002) peaks of CCO, STO and the substrate NGO; b) Finite size effect oscillations of the (001) peak of CCO; c) Finite size effect oscillations of the (002) peak of STO; d) STEM image of the bilayer CCO/STO.

As in CCO/STO superlattices [6], the conductivity, and thus the T_c, of CCO/STO bilayers vary substantially with varying the oxidizing power of the growth atmosphere, from an insulating to a superconducting behaviour with maximum $T_c \approx 40$ K. On the other hand, in bare CCO films, only a slight variation of the resistance has been obtained by changing the oxidizing growth conditions, but no superconducting phase has been revealed (see also Ref.6). This finding clearly indicates that the interface with the STO is the structural feature needed for the occurrence of superconductivity. As previously suggested for the case of CCO/STO superlattices, the doping is supposed to occur thanks to extra oxygen atoms which are introduced in the system during the growth, most probably at the CCO/STO interfaces [6, 8, 9]. However, since in the SL each CCO block is embedded between two STO blocks, two kinds of interface structures are present at the top and at the bottom side of the CCO: CuO_2-Ca-TiO_2-SrO and TiO_2-SrO-CuO_2-Ca, respectively.

The bilayer CCO/STO on NdO-terminated substrate gives us the possibility to discriminate between the two kinds of interfaces (see Fig. 2) and to clarify if one of them is privileged in hosting superconductivity. Indeed, if on the NdO-terminated NGO substrate the CCO is deposited first, resulting in the NGO/CCO/STO heterostructure, the CCO/STO interface presents the following sequence of atomic planes: CuO_2-Ca-TiO_2-SrO (see Fig.2b). Let us name this sequence interface α. On the contrary, if STO is deposited first on NGO and then the CCO on top of STO, to form the heterostructure NGO/STO/CCO, the interface between STO and CCO is TiO_2-SrO-CuO_2-Ca (see Fig.2d). Let us call this stacking interface β. The two different atomic plane sequences, due to the different growth order, have been confirmed by STEM, as shown in the following. In Fig.2a we report the R(T) curves for the two samples with different stacking order. In the case of NGO/CCO/STO the system is superconducting; whereas in the case NGO/STO/CCO no superconductivity is achieved. From these findings we deduce that, most probably, the interface capable to host superconductivity is CuO_2-Ca-TiO_2-SrO (see Fig.2b).

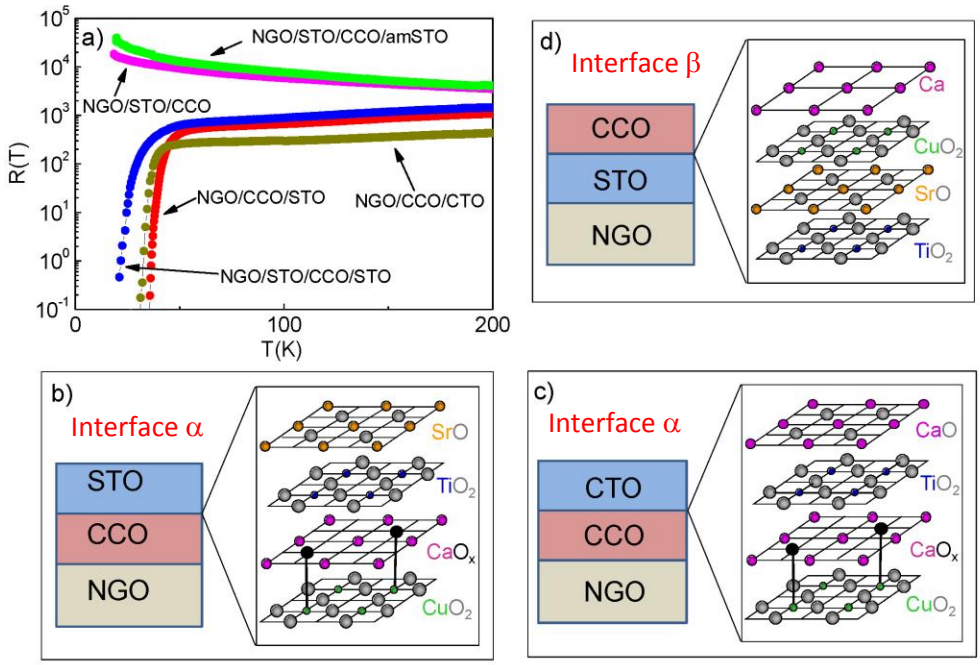

Figure 2: **Transport properties of the bilayers as a function of different stacking sequence**. a) Resistance as a function of temperature for the bilayer NGO/CCO/STO, the bilayer NGO/CCO/CTO, the bilayer NGO/STO/CCO, the trilayer NGO/STO/CCO/STO with the top crystalline STO layer, and the trilayer NGO/STO/CCO/amSTO with the top amorphous STO (amSTO) layer. Then, the schematic interface structures for the bilayers NGO/CCO/STO (b), NGO/CCO/CTO (c) and NGO/STO/CCO (d) are shown. The extra oxygen ions introduced in the Ca plane at the interface in NGO/CCO/STO and NGO/CCO/CTO are shown in black instead of grey, and the corresponding apical coordination with the Cu ions is stressed by a thick black line.

This hypothesis has been further checked by growing a trilayer NGO/STO/CCO/STO, where the first STO block and the CCO block have the same thickness as in the bilayer NGO/STO/CCO, and the top STO block has the same thickness as the STO block in NGO/CCO/STO bilayer. In this trilayer, both interfaces are again present and the superconducting behaviour is recovered (see Fig.2a). Moreover, if the top STO layer in the trilayer is made by amorphous STO (grown at low temperature), instead of crystalline epitaxial STO, the system remains insulating as for the NGO/STO/CCO bilayer (Fig.2a). This further confirms that a sharp CuO_2-Ca-TiO_2-SrO interface is necessary for superconductivity.

A possible explanation is that, when the Ca plane is faced with the TiO_2 plane in the CuO_2-Ca-TiO_2-SrO interface, it can host the extra oxygen ions needed for the hole doping, giving rise to a CaO_x plane, as indicated by the black dots in the interface scheme in Fig.2b. These extra oxygen ions are in the apical position for the Cu lying in the CuO_2 plane below (see thick black line in the same interface scheme of Fig.2b), which is thus doped with holes. On the contrary, in the other interface, TiO_2-SrO-CuO_2-Ca, the SrO plane is already stoichiometrically full of oxygen ions (Fig.2d), and no doping can occur.

To experimentally check this hypothesis, we performed aberration-corrected STEM/EELS measurements on both kinds of interfaces. In Fig.3, we show STEM images of the CCO/STO interface acquired simultaneously using both the annular bright field (ABF) detector (panel a), and the high-angle annular dark field (HAADF) detector (panel b) for a NGO/$(CCO)_9$/$(STO)_{55}$ bilayer grown on NdO terminated NGO substrate, where the CuO_2-Ca-TiO_2-SrO interface is present. In the HAADF images the intensity scales strongly with the atomic number Z and therefore this type of imaging allows for identification of the different atomic columns via the difference in column intensities for all but the ligthest elements. On the other hand, the ABF imaging geometry has been established as a robust technique to observe light atoms including oxygen [14, 15]. Because in ABF imaging the atoms appear dark on a light background, the ABF image in Fig. 3 has been inverted in order to show the atoms as bright spots on a dark background. In order to better visualize both cations and oxygen columns, an overlay of the HAADF image colored in red and the inverted ABF image colored in green is shown in Fig. 3c. In the overlay all the cations appear yellow/orange (overlay of red and green) while the O shows up in green. The intensity profiles of the inverted ABF image, taken at the first (panel e), second (panel f), and fourth (panel g) Ca planes (indicated by the pink, green, and blue arrows, respectively) indicate that a substantial amount of extra oxygen atoms are present only in the Ca plane at the interface with the TiO_2 plane of STO, thus forming a CaO_x plane, whereas no extra oxygen is detected

in the fourth Ca plane. This result reveals that, in these heterostructures, the charge reservoir role is played actually by a *single* atomic plane at the interface. The introduction of excess oxygen atoms only in the Ca plane of CCO at the interface with STO and not in the inner Ca planes can be explained by the presence of strain effect confined at the interface, joined with hybrid nature of the CCO/STO interface. Indeed, depending on the oxygen content x, the interface CaO_x plane can either couple with the CuO_2 plane below to form the infinite layer structure $CaCuO_2$, for the extreme case $x = 0$, or couple with the TiO_2 plane above to form the perovskite structure $CaTiO_3$, for the other extreme case $x = 1$, the latter being a stable compound in the form of film. This opportunity makes the interface Ca plane unique with respect to the inner Ca planes of the CCO.

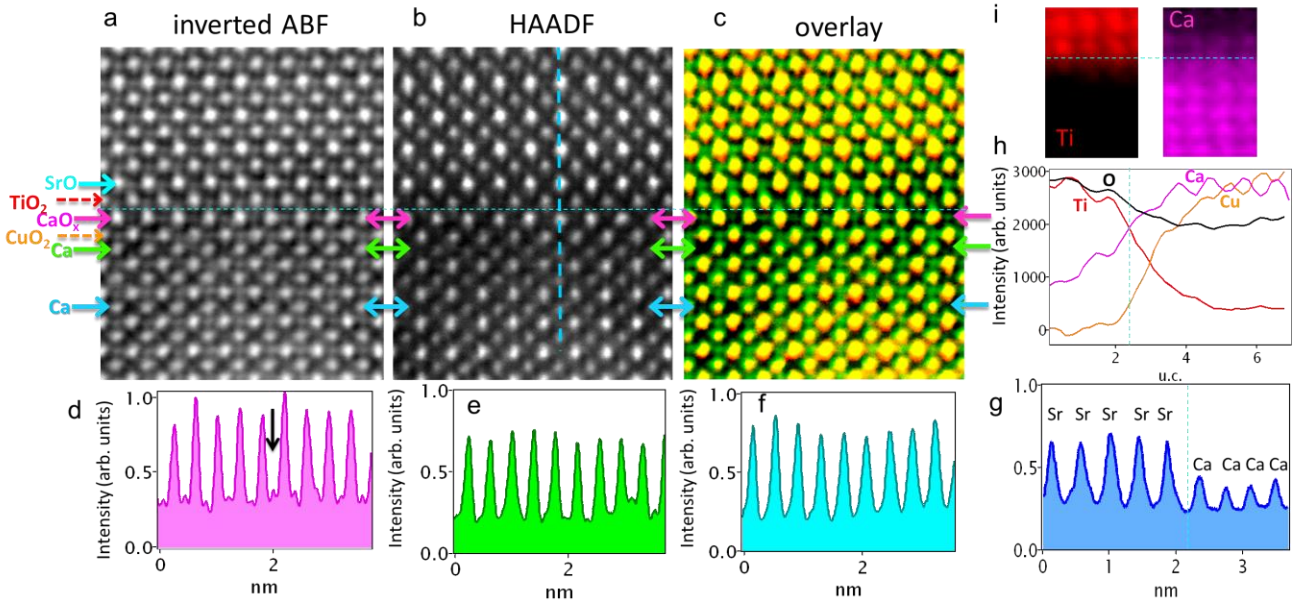

Figure 3: **Structure of the CCO/STO interface**: a) Inverted ABF images showing O columns. b) HAADF image showing cations with Z contrast. c) overlay of (a) in green and (b) in red, showing all the cations in orange (overlay of green and red) and the O columns in green. d), e), and f) are line profiles of the inverted ABF image at the magenta (interface Ca plane), green and blue arrow, respectively, showing apical oxygen at the interface Ca plane (black arrow) and no apical oxygen at the 4th Ca plane from the interface (blue arrow). h). EELS elemental profiles showing that Ca diffuses somewhat into the STO. This is seen also in the intensity profile of the HAADF image (g) (taken from the blue line in (b), which shows slightly smaller (larger) intensity for the last Sr (first Ca) column from the left. i) EELS elemental maps for Ti and Ca. Dashed cyan lines indicate the interface.

In the line profile shown in Fig. 3g, taken from the vertical dashed blue line in the HAADF image (panel b), the intensity of the Sr (Ca) column at the interface is slightly smaller (larger) than for the columns away from the interface, revealing the presence of some Ca/Sr interdiffusion at the interface. This was confirmed by the elemental maps and profiles obtained by EELS and shown in Fig. 3i,h. The EELS maps were obtained by acquiring a spectrum image, that is a set of data comprising an EELS spectrum for each pixel x_i,y_i in the region shown in Fig. 3i. Subsequentely, the integrated intensities of the Ti-$L_{2,3}$, Ca-$L_{2,3}$, Cu-$L_{2,3}$ and O-K edges of each EELS spectrum are plotted for every pixel. The profiles are then obtained by summing the signal within the map in the direction parallel to the interface. However, the occurrence of Ca/Sr interdiffusion is not relevant for the appearance of superconductivity for two main reasons: 1) Ca is isovalent to Sr, therefore, no Sr doping can be envisaged; 2) the bilayer $CaCuO_2/CaTiO_3$, that is, with $CaTiO_3$ (CTO) instead of $SrTiO_3$, and thus with no possibility of Ca/Sr interdiffusion, is also superconducting with similar T_c, as shown in Fig.2a. In this case the interface is CuO_2-Ca-TiO_2-CaO (Fig.2c), therefore with a structure identical to that in NGO/CCO/STO bilayer except for the presence of Ca instead of Sr in the last atomic plane. This last result is important since it generalizes the choice of the non-cuprate block from STO to many other possible insulating oxides. According to the above considerations about the IL/perovskite hybrid character of the CCO/STO interface, we suggest that, among all the possible ABO_3 (ABO) perovkites, the ones yielding superconducting CCO/ABO heterostructures are the ones for which the corresponding $CaBO_3$ compound exists in form of film.

Apart from the Ca diffusion in the STO, which can be also due to resputtering of light cations during ion-mill thinning, the CCO/STO interface is fairly sharp from the point of view of the other cations. Indeed, in the elemental profile (see Fig. 3d), Cu and Ti profiles decay much faster than the Ca profile, indicating that the CuO_2 plane below the interface is almost ideal. This fact can be considered a good condition for the occurrence of superconductivity. Moreover, the peak positions in the line

profiles in panel h confirm the assumed CuO_2-Ca-TiO_2-SrO plane stacking.

The same measurements are shown in Fig.4 for the STO/CCO interface taken on the trilayer STO/CCO/STO. Here, the intensity profiles show that, whereas in the interface SrO plane the oxygen ions are present, as they should in order to complete the neutral unit cell of STO (TiO_2-SrO), in the Ca plane just above, no substantial number of doping oxygen ions is present and this interface is thus not conducting.

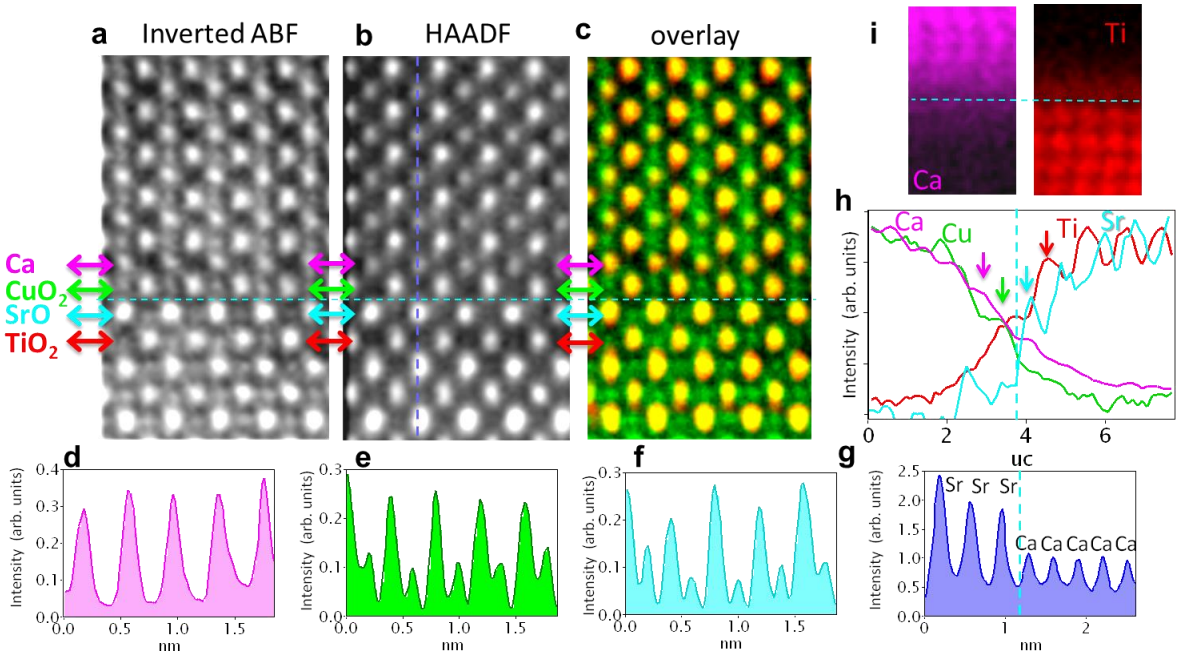

Figure 4: **Structure of the STO/CCO interface**: a) Inverted ABF images. b) HAADF image. c) overlay of (a) in green and (b) in red, showing all the cations in orange and the O columns in green. d), e), and f) are line profiles of the inverted ABF image at the magenta (interface Ca plane), green (CuO2) and blue (SrO) arrows, respectively, showing no oxygen at the interface Ca plane. h). EELS elemental line profiles for Ca, Cu, Ti, and Sr confirming a quite sharp interface with stacking TiO_2-SrO-CuO_2-Ca. g) line profile taken from (b) at the blue line. i) EELS elemental maps for Ti and Ca. Dashed cyan lines indicate the interface position. Arrows in (h) indicate by color coding the stacking of atomic planes at the interface.

On the base of the results shown up to now, we can assume that in CCO/STO heterostructures the doping is a pure interface phenomenon, occurring by the uptaking of extra oxygen atoms in a single Ca plane at the interface and the consequent charge transfer to the CuO_2 planes, one may wonder how

far from the interface the doping holes diffuse within the CCO layer. This, together with the connected dependence of T_c on the number of CuO_2 planes, is also an open question in multilayered HTS [16-22]. Oxygen K-edge X-Ray Absorption spectroscopy has been demonstrated to be a powerful tool to reveal the presence of delocalized holes in HTS [23, 24]. Indeed, a pre-edge feature emerges upon doping HTS, which can be associated to the low-energy quasi-particle band called Zhang-Rice singlet: a locally bound d^9 copper 3d hole hybridized with a doped ligand hole (L) distributed on the planar oxygen 2p orbitals. The same feature can be observed in the EELS spectra at the O K-edge [25,26].

Thanks to the atomic spatial resolution of STEM/EELS, O K-edge spectra could be acquired at different distances from the interface in the trilayer NGO/STO/CCO/STO, where we have two distinct interfaces: the interface with STO at the top (interface α), where extra oxygen ions are present (see Fig. 3), and the interface with STO at the bottom (interface β), where no extra oxygen ions are revealed. In panels a), b) and c) of Fig. 5 the O-K spectra acquired in the STO bulk layers and in the CCO layers close to interface α and to interface β, respectively, are shown. In the vicinity of interface α, the spectrum of the CCO shows a spectral weight, named A in the figure, around 531 eV. This peak disappears on going towards the other interface β and is absent in STO, which is an insulator. According to previous XAS and EELS measurements [23-26], this spectral weight is ascribed to the delocalized doping holes. Namely, peak A results mainly from $3d^9L \rightarrow 1s3d^9$ transitions, where L and 1s denote the O $2p_{x,y}$ ligand hole and O 1s core hole, respectively.

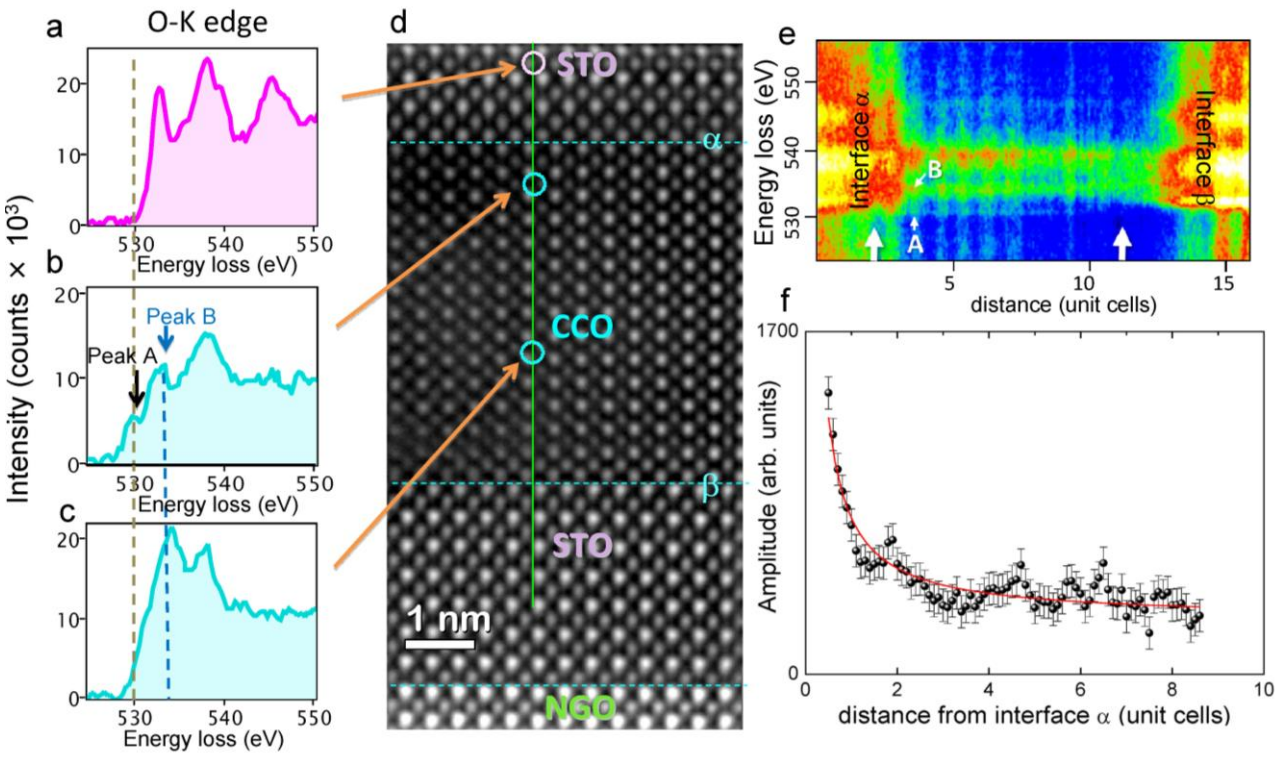

Figure 5: **Variation of the number of doping holes as a function of the distance from the CCO/STO interface in the trilayer NGO/STO/CCO/STO**. a) O-K edge from the upper STO layer in (d). b) O-K edge from the CCO rigth below the STO layer, corresponding to x = 1.2 u.c. in f. c) CCO O-K edge near the bottom STO layer, corresponding to x = 8.5 u.c. in f. spectra a)-c) are shown after background subtraction and noise reduction by principal component analysis (PCA). d) HAADF image of the trilayer sample from which the spectrum image in (e) was taken. e) spectrum image (raw data) showing decreasing peak A amplitude in going from interface α to interface β (big white arrows indicate the range of data shown in f, small white arrows indicate the position of peak A and B as indicated in panel b). f) plot of the amplitude of A as a function of the distance *d* from the top CCO/STO interface. The line is a fit with 1/*d* dependence.

The dependence of the amplitude of peak A on the distance *d* from the top interface α is reported in panel f) of Fig. 5. The holes concentration decays rapidly with the distance from the top interface α and is drastically reduced already in the second CCO unit cell (second CuO_2 plane).

This behavior, with 1/d dependence, as shown by the fit in Fig.5f, can be explained by the presence of an attractive electrostatic potential [19] associated with the negatively charged extra apical oxygen ions localized at the Ca interface plane. According to this result, a purely interfacial nature of

high T_c superconductivity can be deduced. We can, indeed, consider the results shown in Fig.5 a *direct* measurement of the detailed dependence of the holes concentration on the number of CuO_2 planes in the IL block of HTS. From this point of view, the dependence of T_c on the number n of CuO_2 planes in multilayered HTS [16-22], where the CR blocks inject carriers from both the top and the bottom interface (top and bottom interface of IL block with CR blocks are identical in HTS), can be explained. Given the dependence of the holes concentration on the distance from the interface shown in Fig. 5, the doping of the CuO_2 planes in HTS with $n \approx 3$ is homogeneous among the planes and the T_c is maximum. For $n > 3$, the holes diffuse also to inner CuO_2 planes, the doping starts to be lower on average and not homogeneous, and the T_c decreases. For $n \geq$ 4-5, since the holes are confined by the electrostatic shielding within about 1-2 CuO_2 planes close to each interface of the IL block with the CR block, the inner planes are actually less than underdoped, and, most probably, antiferromagnetic, as also suggested in previous NMR studies [19]. Therefore, the increase of n above 5 should not induce any change in T_c, which, indeed, keeps constant [22]. It is significant that for CCO/STO superlattices a T_c vs. n behaviour identical to the one found in HTS is reported [6]. This fact supports the reliability of the similitude between CCO/STO interface and IL/CR interface in HTS.

In conclusion, we have shown that the heterostructure CCO/STO with a single interface is superconducting at high T_c. The doping is achieved thanks to extra oxygen atoms, which, during the growth, are incorporated in the Ca plane of CCO at the interface with STO, giving rise to CaO_x composition of the Ca interface atomic plane. A direct measurement of the concentration of the doping holes, introduced by the extra oxygen, ions as a function of the distance from the charge reservoir interface shows that they are confined within about 1-2 CCO unit cells from the interface with STO. Deeper CuO_2 planes cannot be doped. The same behavior is expected to occur in standard multilayer HTS, where both the IL/CR interfaces are active, thus explaining the dependence of T_c on the number of CuO_2 planes in these system.

We can conclude that the doping of the CuO_2 planes in the IL block is not properly due to a charge transfer phenomenon from a second charge reservoir layer. In fact, it is the interface between the IL cuprate and the second block (regardless of its nature) that plays the crucial role through the uptaking of negatively charged defects. In this scenario the superconducting properties are mostly connected with interface properties, such as termination, sharpness and capability of accommodating a large number of extra charges without diffusion of them toward the cuprate block. Obviously, the non-cuprate block should be electronically inert to avoid charge shielding on the wrong side of the interface. With these clues in mind the search for interfaces with improved superconducting properties can proceed by looking for other non-cuprate blocks having a better lattice match with CCO, a fully controlled termination at the interface and a better capability to accommodate extra oxygen ions.

The results reported in this work have in our opinion also other important implications. Indeed, they show that it is possible, in a relatively easy way, to isolate a single CuO_2 high T_c superconducting plane. This is considered an important step towards the achievement of resistance-free electrical transport in 2D channels [28]. Indeed, this is connected to the possibility to realize new superconducting field effect devices, operating at temperatures much higher than the ones realized with the LAO/STO heterostructure [7, 23], with also the possibility to tune the thickness of the STO dielectric for top-gated devices.

Methods

Sample preparation. We used the pulsed laser deposition technique (KrF excimer laser, λ = 248 nm) to synthesize all the CCO/STO samples studied in this work. The substrate used for the film deposition is 5x5 mm^2 $NdGaO_3$ (110), whose NdO termination has been obtained by annealing in air for about two hours at 1000 °C [29]. Two targets, with $CaCuO_2$ and $SrTiO_3$ nominal composition, mounted on a multitarget system, were used. The STO target is a commercial crystal obtained from Crystal, GmbH.

The CCO target was prepared by standard solid state reaction, according to the following procedure: stoichiometric mixtures of high-purity $CaCO_3$ and CuO powders were calcined at 860 °C in air for 24 h, pressed to form a disk, and finally heated at 900 °C for 12 h. The substrate was placed at a distance 2.2 cm from the targets on a heated holder and its temperature during the deposition of the films was $T \approx 600$ °C (see also Ref. [6]). To obtain superconducting heterostructures, the deposition chamber is first evacuated down to P ~ 10^{-5} mbar and then a mixture of oxygen and 12% ozone atmosphere at a pressure of about 1 mbar is used for the growth, in order to obtain a strongly oxidizing atmosphere. At the end of the deposition, films were cooled down at the growth pressure. Bilayers CCO/STO with CCO and STO thickness ranging from 10 to 60 unit cells were grown.

Transport and structural characterization. The transport properties were measured by the four-probe dc technique in the Van der Pauw geometry, so that the measured resistance R is given by $R = R_s \cdot \ln 2/\pi$, where R_s is the sheet resistance. Four small contacts were made by silver epoxy directly at the corners of the square substrate before the film deposition, in order to avoid any chemical reaction between the film and the solvent utilized in the silver epoxy. Basic structural characterization is realized by Co K_α x-ray diffraction measurements in a θ-2θ Bragg-Brentano geometry.

STEM/EELS measurements. Simultaneous spectroscopy, high angle annular dark field (HAADF) and annular bright field (ABF) imaging was conducted on five different bilayer and trilayer samples that were thinned to electron transparency in cross sectional geometry, using conventional polishing and ion milling techniques. The microscopes used for this study were a Nion UltraSTEM 100TM operating at 100 kV [30] and a Nion UltraSTEM 200TM microscope operating at 200 kV [31]. Both microscopes are equipped with a second generation 5th order probe aberration corrector, a cold field emission electron gun, and a Gatan EEL spectrometer (Enfina, and Enfinium for the 100 kV and the 200 kV, respectively) The 200 kV microscope routinely achieves a spatial resolution of 0.6 Å and was mainly used for HAADF and ABF imaging . HAADF and ABF inner collection half-angles were 68

and 11 mrad, respectively. The probe convergence half angle was 30 mrad. The maximum EELS energy resolution was 300 meV, and the EELS collection angle was 48 mrad. For studying the profile of doping holes, which required high signal to noise ratio and high energy resolution, linear spectrum images were acquired with dwelling time of 0.5 s and a dispersion of 0.1 eV/ch..

References

[1] Hwang, H. Y. Atomic control of the electronic structure at complex oxide heterointerfaces. *Mater. Res. Soc. Bull.* **31**, 28–35 (2006).

[2] Ohtomo, A. H., Wang, H.Y. A high-mobility electron gas at the $LaAlO_3/SrTiO_3$ heterointerface. *Nature* **427**, 423 (2004).

[3] Tsukazaki, A. *et al.* Quantum Hall effect in polar oxide heterostructures. *Science* **315,** 1388 (2007).

[4] Reyren, N. *et al.* Superconducting interfaces between insulating oxides. *Science* **317**, 1196-1199 (2007).

[5] Gozar, A. *et al.* High-temperature interface superconductivity between metallic and insulating copper oxides. *Nature* **455,** 782 (2008).

[6] Di Castro, D. *et al.* Occurrence of a high-temperature superconducting phase in $(CaCuO_2)_n/(SrTiO_3)_m$ superlattices. *Phys. Rev. B* **86**, 134524 (2012)

[7] Caviglia, A. D. *et al.* Electric field control of the $LaAlO_3/SrTiO_3$ interface ground state. *Nature* **456**, 624 (2008).

[8] Di Castro, D. *et al.* T_c up to 50 K in superlattices of insulating oxides. *Supercond. Sci. Technol*. **27,** 044016 (2014)

[9] Aruta, C. *et al.* Interface reconstruction in superconducting $CaCuO_2/SrTiO_3$ superlattices: a hard x-ray photoelectron spectroscopy study.*Phys. Rev. B* **87**, 155145 (2013)

[10] Salvato, M. *et al.* Superconducting anisotropy in $(CaCuO_2)_n/(SrTiO_3)_m$ superlattices. *J. Phys.: Condens. Matter* **25** 335702 (2013)

[11] Balestrino, G., Martellucci, S., Medaglia, P. G., Paoletti, A., and Petrocelli, G. Dependence of the critical temperature on *n* in $(BaCuO_2)_2/(CaCuO_2)_n$ superlattices. *Phys. Rev. B* **58**, R8925 (1998)

[12] Aruta, C. *et al.* Hole redistribution across interfaces in superconducting cuprate superlattices. *Phys. Rev. B* **78**, 205120 (2008).

[13] Balestrino, G. Growth of $CaCuO_2$ and $Sr_xCa_{1-x}CuO_2$ epitaxial films on $NdGaO_3$ substrates by pulsed laser deposition. *J. Mater. Chem.* **5**, 1879 (1995).

[14] S.D. Findlay *et al.* Robust atomic resolution imaging of light elements using scanning transmission electron microscopy. *Appl. Phys. Lett.* **95**, 191913 (2009)

[15] Okunishi, E., Sawada, H., Kondo, Y. Experimental study of annular bright field (ABF) imaging using aberration-corrected scanning transmission electron microscopy (STEM). *Micron* **43,** 538–544 (2012)

[16] Scott, B. A. *et al.* Layer dependence of the superconducting transition temperature of $HgBa_2Can_{-1}CunO_2n_{+2+}\delta$. *Physica C* **230**, 239–245 (1994).

[17] Tokunaga, Y. *et al.* Carrier distribution and superconductivity in multilayer high-T_c cuprates proved by ^{63}Cu NMR. *J. Low Temp. Phys*. **117,** 473 (1999).

[18] Tokunaga, Y. *et al.* Effect of carrier distribution on superconducting characteristics of the multilayered high-T_c cuprate $(Cu_{0.6}C_{0.4})Ba_2Ca_3Cu_4O_{12+y}$: ^{63}Cu−NMR study. *Phys. Rev. B* **61,** 9707 (2000).

[19] Kotegawa, H. NMR study of carrier distribution and superconductivity in multilayered high-T_c cuprates. *J. Phys. Chem. Solids* **62**, 171 (2001).

[20] Hamada, N., Ihara, H. Electronic band structures of $CuBa_2Ca_{n-1}Cu_nO_{2n+2}$ and $CuBa_2Ca_{n-1}Cu_nO_{2n+1}F$ (n=3–5). *Physica C* **357–360** 108 (2001).

[21] Chakravarty, S., Kee, H-Y, Voelker, K. An explanation for a universality of transition temperatures in families of copper oxide superconductors, *Nature* **428**, 53 (2004)

[22] A. Iyo *et al.* Synthesis and physical properties of multilayered cuprates. *Physica C* **445 -448**, 17-22 (2006)

[23] Chen, T. *et al.* Electronic states in La2−xSrxCuO4+δ probed by soft-x-ray absorption. *Phys. Rev. Lett*. **66**, 104 (1991)

[24] Chen, C. T., Out-of-plane orbital characters of intrinsic and doped holes in $La_{2-x}Sr_xCuO_4$. *Phys. Rev. Lett.* **68**, 2543 (1992).

[25] Romberg, H., Alexander, M., Nucker, N., Adelmann, P. and Fink, J. Electronic structure of the system $La_{2-x}Sr_xCuO_{4+\delta}$. *Phys. Rev. B* **42**, 8768R (1990)

[26] Gauquelin, N. *et al*. Atomic scale real-space mapping of holes in $YBa_2Cu_3O_{6+\delta}$. *Nature Communications* **5**, 4275 (2014)

[27] Thiel, S., Hammerl, G., Schmehl, A., Schneider, C.W., Mannhart, J. Tunable Quasi-Two-Dimensional Electron Gases in Oxide Heterostructures. *Science* **313**, 1942 (2006).

[28] Gariglio, S., Gabay, M., and Triscone, J-M., Superconductivity on the other side. *Nature nanotechnology* **5**, 13 (2010)

[29] Ohnishi, T. *et al.* A-site layer terminated perovskite substrate: $NdGaO_3$. *Appl. Phys. Lett*. **74**, 2531

(1999).

[30] Krivanek, O.L. *et al.* An electron microscopy for the aberration-corrected era. *Ultramicroscopy* **108,** 179 (2008)

[31] Dellby, N. *et al.* Dedicated STEM for 200 to 40 keV operation. *Eur. Phys. J-Appl. Phys*. **54**, 33505 (2011).

Acknowledgement. This work was partially supported by Italian MIUR (PRIN Project 2010-2011 OXIDE, "OXide Interfaces: emerging new properties, multifunc-tionality, and Devices for Electronics and Energy". CC was supported by the U.S. Department of Energy, Office of Science, Basic Energy Sciences, Materials Sciences and Engineering Division. CC was supported by the U.S. Department of Energy, Office of Science, Basic Energy Sciences, Materials Sciences and Engineering Division, and through a user project supported by ORNL's Center for Nanophase Materials Sciences (CNMS), which is sponsored by the Scientific User Facilities Division, Office of Basic Energy Sciences, U.S. Department of Energy.